

# Observation of Nuclear Scaling in the $A(e, e')$ Reaction at $x_B > 1$

K.Sh. Egiyan,<sup>1</sup> N.Dashyan,<sup>1</sup> M. Sargsian,<sup>11</sup> S. Stepanyan,<sup>36</sup> L.B. Weinstein,<sup>27</sup> G. Adams,<sup>31</sup> P. Ambrozewicz,<sup>11</sup>  
 E. Anciant,<sup>6</sup> M. Anghinolfi,<sup>16</sup> B. Asavapibhop,<sup>23</sup> G. Asryan,<sup>1</sup> G. Audit,<sup>6</sup> T. Auger,<sup>6</sup> H. Avakian,<sup>36</sup>  
 H. Bagdasaryan,<sup>27</sup> J.P. Ball,<sup>2</sup> S. Barrow,<sup>12</sup> M. Battaglieri,<sup>16</sup> K. Beard,<sup>20</sup> I. Bedlinski,<sup>19</sup> M. Bektasoglu,<sup>26</sup>  
 M. Bellis,<sup>31</sup> N. Benmouna,<sup>13</sup> B.L. Berman,<sup>13</sup> N. Bianchi,<sup>15</sup> A.S. Biselli,<sup>4</sup> S. Boiarinov,<sup>19</sup> B.E. Bonner,<sup>32</sup>  
 S. Bouchigny,<sup>17</sup> R. Bradford,<sup>4</sup> D. Branford,<sup>10</sup> W.J. Briscoe,<sup>13</sup> W.K. Brooks,<sup>36</sup> V.D. Burkert,<sup>36</sup> C. Butuceanu,<sup>40</sup>  
 J.R. Calarco,<sup>24</sup> D.S. Carman,<sup>4</sup> B. Carnahan,<sup>5</sup> C. Cetina,<sup>13</sup> L. Ciciani,<sup>27</sup> P.L. Cole,<sup>35</sup> A. Coleman,<sup>40</sup> D. Cords,<sup>36</sup>  
 P. Corvisiero,<sup>16</sup> D. Crabb,<sup>39</sup> H. Crannell,<sup>5</sup> J.P. Cummings,<sup>31</sup> E. DeSanctis,<sup>15</sup> R. DeVita,<sup>16</sup> P.V. Degtyarenko,<sup>36</sup>  
 R. Demirchyan,<sup>1</sup> H. Denizli,<sup>29</sup> L. Dennis,<sup>12</sup> K.V. Dharmawardane,<sup>27</sup> K.S. Dhuga,<sup>13</sup> C. Djalali,<sup>34</sup> G.E. Dodge,<sup>27</sup>  
 D. Doughty,<sup>7</sup> P. Dragovitsch,<sup>12</sup> M. Dugger,<sup>2</sup> S. Dytman,<sup>29</sup> O.P. Dzyubak,<sup>34</sup> M. Eckhause,<sup>40</sup> H. Egiyan,<sup>36</sup>  
 L. Elouadrhiri,<sup>36</sup> A. Empl,<sup>31</sup> P. Eugenio,<sup>12</sup> R. Fatemi,<sup>39</sup> R.J. Feuerbach,<sup>4</sup> J. Ficenec,<sup>38</sup> T.A. Forest,<sup>27</sup> H. Funsten,<sup>40</sup>  
 M. Gai,<sup>8</sup> G. Gavalian,<sup>24</sup> S. Gilad,<sup>22</sup> G.P. Gilfoyle,<sup>33</sup> K.L. Giovanetti,<sup>20</sup> P. Girard,<sup>34</sup> C.I.O. Gordon,<sup>14</sup> K. Griffioen,<sup>40</sup>  
 M. Guidal,<sup>17</sup> M. Guillo,<sup>34</sup> L. Guo,<sup>36</sup> V. Gyurjyan,<sup>36</sup> C. Hadjidakis,<sup>17</sup> R.S. Hakobyan,<sup>5</sup> J. Hardie,<sup>7</sup> D. Heddle,<sup>7</sup>  
 P. Heimberg,<sup>13</sup> F.W. Hersman,<sup>24</sup> K. Hicks,<sup>26</sup> R.S. Hicks,<sup>23</sup> M. Holtrop,<sup>24</sup> J. Hu,<sup>31</sup> C.E. Hyde-Wright,<sup>27</sup> Y. Ilieva,<sup>13</sup>  
 M.M. Ito,<sup>36</sup> D. Jenkins,<sup>38</sup> K. Joo,<sup>36</sup> J.H. Kelley,<sup>9</sup> M. Khandaker,<sup>25</sup> D.H. Kim,<sup>21</sup> K.Y. Kim,<sup>29</sup> K. Kim,<sup>21</sup> M.S. Kim,<sup>21</sup>  
 W. Kim,<sup>21</sup> A. Klein,<sup>27</sup> F.J. Klein,<sup>36</sup> A. Klimenko,<sup>27</sup> M. Klusman,<sup>31</sup> M. Kossov,<sup>19</sup> L.H. Kramer,<sup>11</sup> Y. Kuang,<sup>40</sup>  
 S.E. Kuhn,<sup>27</sup> J. Kuhn,<sup>4</sup> J. Lachniet,<sup>4</sup> J.M. Laget,<sup>6</sup> D. Lawrence,<sup>23</sup> Ji Li,<sup>31</sup> K. Lukashin,<sup>36</sup> J.J. Manak,<sup>36</sup>  
 C. Marchand,<sup>6</sup> L.C. Maximon,<sup>13</sup> S. McAleer,<sup>12</sup> J. McCarthy,<sup>39</sup> J.W.C. McNabb,<sup>4</sup> B.A. Mecking,<sup>36</sup>  
 S. Mehrabyan,<sup>29</sup> J.J. Melone,<sup>14</sup> M.D. Mestayer,<sup>36</sup> C.A. Meyer,<sup>4</sup> K. Mikhailov,<sup>19</sup> R. Minehart,<sup>39</sup> M. Mirazita,<sup>15</sup>  
 R. Miskimen,<sup>23</sup> L. Morand,<sup>6</sup> S.A. Morrow,<sup>6</sup> M.U. Mozer,<sup>26</sup> V. Muccifora,<sup>15</sup> J. Mueller,<sup>29</sup> L.Y. Murphy,<sup>13</sup>  
 G.S. Mutchler,<sup>32</sup> J. Napolitano,<sup>31</sup> R. Nasseripour,<sup>11</sup> S.O. Nelson,<sup>9</sup> S. Niccolai,<sup>13</sup> G. Niculescu,<sup>26</sup> I. Niculescu,<sup>20</sup>  
 B.B. Niczyporuk,<sup>36</sup> R.A. Niyazov,<sup>27</sup> M. Nozar,<sup>36</sup> G.V. O'Rielly,<sup>13</sup> A.K. Opper,<sup>26</sup> M. Osipenko,<sup>16</sup> K. Park,<sup>21</sup>  
 E. Pasyuk,<sup>2</sup> G. Peterson,<sup>23</sup> S.A. Philips,<sup>13</sup> N. Pivnyuk,<sup>19</sup> D. Pocanic,<sup>39</sup> O. Pogorelko,<sup>19</sup> E. Polli,<sup>15</sup>  
 S. Pozdniakov,<sup>19</sup> B.M. Preedom,<sup>34</sup> J.W. Price,<sup>3</sup> Y. Prok,<sup>39</sup> D. Protopopescu,<sup>14</sup> L.M. Qin,<sup>27</sup> B.A. Raue,<sup>11</sup>  
 G. Riccardi,<sup>12</sup> G. Ricco,<sup>16</sup> M. Ripani,<sup>16</sup> B.G. Ritchie,<sup>2</sup> F. Ronchetti,<sup>15</sup> P. Rossi,<sup>15</sup> D. Rowntree,<sup>22</sup> P.D. Rubin,<sup>33</sup>  
 F. Sabatié,<sup>6</sup> K. Sabourov,<sup>9</sup> C. Salgado,<sup>25</sup> J.P. Santoro,<sup>38</sup> V. Sapunenko,<sup>16</sup> R.A. Schumacher,<sup>4</sup> V.S. Serov,<sup>19</sup>  
 A. Shafi,<sup>13</sup> Y.G. Sharabian,<sup>1</sup> J. Shaw,<sup>23</sup> S. Simionatto,<sup>13</sup> A.V. Skabelin,<sup>22</sup> E.S. Smith,<sup>36</sup> L.C. Smith,<sup>39</sup>  
 D.I. Sober,<sup>5</sup> M. Spraker,<sup>9</sup> A. Stavinsky,<sup>19</sup> P. Stoler,<sup>31</sup> I. Strakovsky,<sup>13</sup> S. Strauch,<sup>13</sup> M. Strikman,<sup>28</sup>  
 M. Taiuti,<sup>16</sup> S. Taylor,<sup>32</sup> D.J. Tedeschi,<sup>34</sup> U. Thoma,<sup>36</sup> R. Thompson,<sup>29</sup> L. Todor,<sup>4</sup> C. Tur,<sup>34</sup> M. Ungaro,<sup>31</sup>  
 M.F. Vineyard,<sup>37</sup> A.V. Vlassov,<sup>19</sup> K. Wang,<sup>39</sup> A. Weisberg,<sup>26</sup> H. Weller,<sup>9</sup> D.P. Weygand,<sup>36</sup> C.S. Whisnant,<sup>34</sup>  
 E. Wolin,<sup>36</sup> M.H. Wood,<sup>34</sup> L. Yanik,<sup>13</sup> A. Yegneswaran,<sup>36</sup> J. Yun,<sup>27</sup> B. Zhang,<sup>22</sup> J. Zhao,<sup>22</sup> and Z. Zhou<sup>22</sup>

(The CLAS Collaboration)

<sup>1</sup> Yerevan Physics Institute, Yerevan 375036, Armenia

<sup>2</sup> Arizona State University, Tempe, Arizona 85287-1504

<sup>3</sup> University of California at Los Angeles, Los Angeles, California 90095-1547

<sup>4</sup> Carnegie Mellon University, Pittsburgh, Pennsylvania 15213

<sup>5</sup> Catholic University of America, Washington, D.C. 20064

<sup>6</sup> CEA-Saclay, Service de Physique Nucléaire, F91191 Gif-sur-Yvette, Cedex, France

<sup>7</sup> Christopher Newport University, Newport News, Virginia 23606

<sup>8</sup> University of Connecticut, Storrs, Connecticut 06269

<sup>9</sup> Duke University, Durham, North Carolina 27708-0305

<sup>10</sup> Edinburgh University, Edinburgh EH9 3JZ, United Kingdom

<sup>11</sup> Florida International University, Miami, Florida 33199

<sup>12</sup> Florida State University, Tallahassee, Florida 32306

<sup>13</sup> The George Washington University, Washington, DC 20052

<sup>14</sup> University of Glasgow, Glasgow G12 8QQ, United Kingdom

<sup>15</sup> INFN, Laboratori Nazionali di Frascati, Frascati, Italy

<sup>16</sup> INFN, Sezione di Genova, 16146 Genova, Italy

<sup>17</sup> Institut de Physique Nucleaire ORSAY, Orsay, France

<sup>18</sup> Institute für Strahlen und Kernphysik, Universität Bonn, Germany

<sup>19</sup> Institute of Theoretical and Experimental Physics, Moscow, 117259, Russia

<sup>20</sup> James Madison University, Harrisonburg, Virginia 22807

<sup>21</sup> Kungpook National University, Taegu 702-701, South Korea

- <sup>22</sup> Massachusetts Institute of Technology, Cambridge, Massachusetts 02139-4307  
<sup>23</sup> University of Massachusetts, Amherst, Massachusetts 01003  
<sup>24</sup> University of New Hampshire, Durham, New Hampshire 03824-3568  
<sup>25</sup> Norfolk State University, Norfolk, Virginia 23504  
<sup>26</sup> Ohio University, Athens, Ohio 45701  
<sup>27</sup> Old Dominion University, Norfolk, Virginia 23529  
<sup>28</sup> Pennsylvania State University, State Collage, Pennsylvania 16802  
<sup>29</sup> University of Pittsburgh, Pittsburgh, Pennsylvania 15260  
<sup>30</sup> Università di ROMA III, 00146 Roma, Italy  
<sup>31</sup> Rensselaer Polytechnic Institute, Troy, New York 12180-3590  
<sup>32</sup> Rice University, Houston, Texas 77005-1892  
<sup>33</sup> University of Richmond, Richmond, Virginia 23173  
<sup>34</sup> University of South Carolina, Columbia, South Carolina 29208  
<sup>35</sup> University of Texas at El Paso, El Paso, Texas 79968  
<sup>36</sup> Thomas Jefferson National Accelerator Facility, Newport News, Virginia 23606  
<sup>37</sup> Union College, Schenectady, NY 12308  
<sup>38</sup> Virginia Polytechnic Institute and State University, Blacksburg, Virginia 24061-0435  
<sup>39</sup> University of Virginia, Charlottesville, Virginia 22901  
<sup>40</sup> College of William and Mary, Williamsburg, Virginia 23187-8795

(Dated: October 31, 2018)

The ratios of inclusive electron scattering cross sections of  ${}^4\text{He}$ ,  ${}^{12}\text{C}$ , and  ${}^{56}\text{Fe}$  to  ${}^3\text{He}$  have been measured for the first time. It is shown that these ratios are independent of  $x_B$  at  $Q^2 > 1.4$  ( $\text{GeV}/c$ )<sup>2</sup> for  $x_B > 1.5$  where the inclusive cross section depends primarily on the high-momentum components of the nuclear wave function. The observed scaling shows that the momentum distributions at high-momenta have the same shape for all nuclei and differ only by a scale factor. The observed onset of the scaling at  $Q^2 > 1.4$  and  $x_B > 1.5$  is consistent with the kinematical expectation that two nucleon short range correlations (SRC) are dominate the nuclear wave function at  $p_m \gtrsim 300$  MeV/c. The values of these ratios in the scaling region can be related to the relative probabilities of SRC in nuclei with  $A \geq 3$ . Our data demonstrate that for nuclei with  $A \geq 12$  these probabilities are 5-5.5 times larger than in deuterium, while for  ${}^4\text{He}$  it is larger by a factor of about 3.5.

PACS numbers: PACS : 13.60.Le, 13.40.Gp, 14.20.Gk

## I. INTRODUCTION

Due to the strong interaction and short distances between the nucleons in nuclei, there is a significant probability for nucleon wave functions to overlap, resulting in short range nucleon-nucleon correlations (SRC) in nuclei [1]. Investigation of SRC is important for at least two reasons. First, because of the short range nature of these correlations, they should contribute significantly to the high-momentum component of the nuclear wave function. Second, scattering from nucleons in SRC will provide unique data on the modification of deeply bound nucleons, which is extremely important for a complete understanding of nucleon structure in general.

High-energy inclusive electron scattering from nuclei,  $A(e, e')$ , is one of the simplest ways to investigate SRC. In particular, it is probably the best way to measure the probabilities of SRC in nuclei. The main problem in these studies is selecting the electron-SRC scattering events from the orders-of-magnitude larger background of inelastic and/or quasi-elastic interaction of electrons with the uncorrelated low-momentum nucleons.

By measuring cross sections at

$$x_B = \frac{Q^2}{2M\nu} > 1, \quad (1)$$

contributions from inelastic electron-nucleon scattering

and meson exchange currents (at high  $Q^2$ ) can be significantly reduced, which corresponds to studying the low-energy-loss side of the quasi-elastic peak. In Eq. 1  $Q^2$  is the four-momentum squared of the virtual photon ( $Q^2 = -q^\mu q_\mu > 0$ ),  $\nu$  is the energy transfer,  $x_B$  is the Bjorken scaling variable, and  $M$  is the nucleon mass,

Many previous analyses of data in this kinematic region concentrate on using  $y$ -scaling to study nucleon momentum distributions (see *e.g.* Refs. [2], [3]). While this technique provides some information about the nuclear wave function, it does not measure the probability of finding SRC in nuclei.

Meanwhile, the data at  $x_B > 1$  can be used to measure the probability of finding SRC in nuclei. There are theoretical predictions that at momenta higher than the Fermi momentum, the nucleon momentum distributions in light and heavy nuclei are similar (see *e.g.* Ref. [4]). This implies that they originate predominantly from the interaction between two nearby nucleons, *i.e.* due to SRC. If the  $A(e, e')$  cross section depends primarily on the nuclear wave function and the shape of this wave function at high-momentum is really universal, then in this high-momentum region the ratio of weighted ( $e, e'$ ) cross sections for different nuclei [34] should scale, *i.e.* they should be independent of electron scattering variables ( $Q^2$  and  $x_B$ ), with the magnitude of the scaling factor being proportional to the relative probability of

SRC in the two nuclei [5, 6].

In Ref. [6] this was checked by analyzing existing SLAC  $A(e, e')$  data for deuterium [7, 8, 9] and heavier nuclei [10]. They found an indication of scaling at  $Q^2 > 1$  and  $x_B \geq 1.5$ . However, since the data for deuterium and the heavy nuclei were collected in different experiments at similar  $Q^2$  but at different electron scattering angles and incident electron energies, to find the ratios at the same values of  $(x_B, Q^2)$ , a complicated fitting and interpolation procedure was applied [6] to the data. The main problem was that the cross sections varied very strongly with angle, incident energy, and  $Q^2$ . To simplify the interpolation, the electron-deuteron cross section was first divided by the theoretical calculation within the impulse approximation. Therefore, the data are not purely experimental, since they include the theoretical calculations, and the ratios may have been affected by the fitting and interpolation procedures.

In this work, the yields of the reaction  $A(e, e')$  for  ${}^3\text{He}$ ,  ${}^4\text{He}$ ,  ${}^{12}\text{C}$ , and  ${}^{56}\text{Fe}$  targets are measured in the same kinematical conditions, and the ratios  $A(e, e')/{}^3\text{He}(e, e')$  are obtained for  $1 < x_B < 2$  and  $Q^2 > 0.65$  (GeV/c) $^2$ . Furthermore, using the scaling behavior of these ratios, the relative probability of  $NN$  SRC for the various nuclei have been extracted.

## II. KINEMATICS AND PREDICTIONS

In order to suppress the background from quasi-elastic interactions of electrons with the uncorrelated low-momentum nucleons (see Fig. 1a), we further restrict the kinematic variables  $x_B$  and  $Q^2$ .

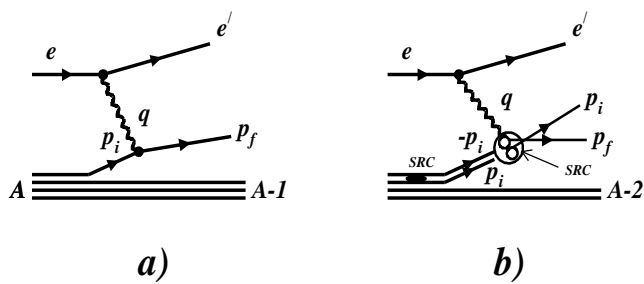


FIG. 1: Two mechanisms of  $A(e, e')$  scattering. a) single nucleon model; b) Short Range Correlation model.

For quasi-elastic  $A(e, e')$  scattering,  $x_B$ ,  $Q^2$ , and the minimum  $A - 1$  recoil momentum contributing to the reaction are related by energy and momentum conservation:

$$(q + p_A - p_{A-1})^2 = p_f^2 = m_N^2, \quad (2)$$

where  $q$ ,  $p_A$ ,  $p_{A-1}$ , and  $p_f$  are the four-momenta of the virtual photon, target nucleus, residual  $A-1$  system, and knocked-out nucleon respectively (note that only  $q$  and

$p_A$  are known.) From Eq.(2) one obtains:

$$\Delta M^2 - Q^2 + \frac{Q^2}{m_N x_B} \left( M_A - \sqrt{M_{A-1}^2 + \vec{p}_m^2} \right) - 2\vec{q} \cdot \vec{p}_m - 2M_A \sqrt{M_{A-1}^2 + \vec{p}_m^2} = 0, \quad (3)$$

where  $\Delta M^2 = M_A^2 + M_{A-1}^2 - m_N^2$  and  $\vec{p}_m = \vec{p}_f - \vec{q} = -\vec{p}_{A-1}$  is the recoil momentum involved in the reaction (sometimes referred to as the ‘missing momentum’ in  $(e, e')p$  reactions). Eq. (3) defines a simple relationship between  $|\vec{p}_m^{min}|$  and  $x_B$  at fixed  $Q^2$ . This relation for deuterium at various values of  $Q^2$  is shown in Fig. 2a. Fig. 2b shows the same relationship for various nuclei at  $Q^2 = 2$  (GeV/c) $^2$ . Note that this relationship is different for the different nuclei, due primarily to differences in the mass of the recoil  $A - 1$  system. This minimum recoil momentum is one of the possible definitions of the scaling variable  $y$ .

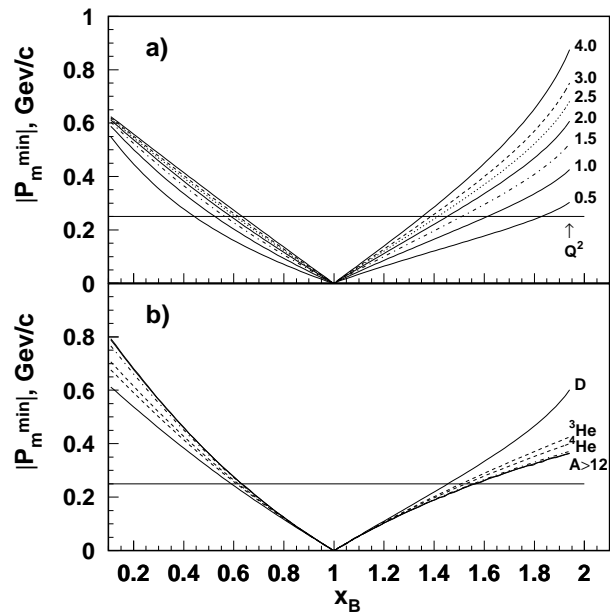


FIG. 2: The minimum recoil momentum as a function of  $x_B$ . a) For deuterium at several  $Q^2$  (in (GeV/c) $^2$ ); b) For different nuclei at  $Q^2 = 2.0$  (GeV/c) $^2$ . Horizontal lines at 250 MeV/c indicate the Fermi momentum typical of the uncorrelated motion of nucleons in nuclei.

One can see from Fig.2 that for any nucleus  $A$  and fixed  $Q^2$ , we can find the value  $x_B^0$  such that at  $x_B > x_B^0$  the magnitude of the minimum recoil momentum,  $|\vec{p}_m^{min}|$ , contributing to the reaction, exceeds the average Fermi momentum in nucleus  $A$ .

It should be pointed out that the initial momentum of the struck nucleon  $\vec{p}_i$  is equal to  $\vec{p}_m$  only in the simplest model where the virtual photon is absorbed on one nucleon and that nucleon leaves the nucleus without further interactions (the Plane Wave Impulse Approximation). In reality, the  $(e, e')$  reaction effectively integrates over

many values of  $p_m \geq p_m^{min}$ . In addition, this simple relation between recoil momentum and initial momentum is modified by Final State Interactions (FSI) and the excitation energy of the residual nucleus. These make it difficult to determine the nuclear wave function directly from  $(e, e')$  cross sections. However, for our purposes, it is sufficient to know that when the minimum recoil momentum contributing to the reaction is much larger than the Fermi momentum, the initial momentum of the struck nucleon will also be larger.

Let us now consider various predictions of the ratios of weighted  $(e, e')$  cross sections for different nuclei. In the mechanism for inclusive  $(e, e')$  scattering at  $x_B > 1$  with virtual photon absorption on a single nucleon and the  $A - 1$  system recoiling intact without FSI (see Fig. 1a), the minimum recoil momentum for different nuclei at fixed  $Q^2$  differs and this difference increases with  $x_B$  (see Fig. 2). Therefore, the cross section ratio between different nuclei will increase with  $x_B$  and will not scale.

In the Short Range Correlations model of Frankfurt and Strikman [1] (see Fig. 1b) the high-momentum part of the nuclear momentum distribution is due to correlated nucleon pairs. This means that when the electron scatters from a high-momentum nucleon in the nucleus, we can consider this scattering as an electron-deuterium interaction with the spectator  $A - 2$  system almost at rest. Therefore, according to Fig. 2a, starting from some threshold  $x_B^0$  for fixed  $Q^2$  the cross section ratio

$$R_{A_2}^{A_1}(Q^2, x_B) = \frac{\sigma_{A_1}(Q^2, x_B)/A_1}{\sigma_{A_2}(Q^2, x_B)/A_2}, \quad (4)$$

where  $\sigma_{A_1}$  and  $\sigma_{A_2}$  are the inclusive electron scattering cross sections from nuclei with atomic numbers  $A_1$  and  $A_2$  respectively, will scale (will be constant). Scaling results from the dominance of SRC in the high-momentum component of the nuclear wave function, and it should be observed, for example, for the cross section ratios of heavy nuclei to light nuclei such as  ${}^3\text{He}$ .

Fig. 3a shows  $R_{{}^3\text{He}}^{{}^{12}\text{C}}$ , for  $A_1 = {}^{12}\text{C}$  and  $A_2 = {}^3\text{He}$ , as a function of  $x_B$  for  $Q^2$  from 1.5 to 2.5  $(\text{GeV}/c)^2$  calculated in the SRC model [11]. The ratio for  $A_1 = {}^{56}\text{Fe}$  and  $A_2 = {}^3\text{He}$  is shown in Fig. 3b. The calculations used the Faddeev wave function for  ${}^3\text{He}$  calculated using the Bonn  $NN$  potential [12]. The momentum distributions for heavier nuclei have been modeled through a two component of momentum distribution using mean field distributions for small nucleon momenta and using the deuteron momentum distribution for  $p > 250$  MeV/c, scaled by factor  $a_2(A)$ , per-nucleon probability of  $NN$  SRC in nucleus  $A$ , estimated from Ref. [6]. The mean field momentum distributions used the Harmonic Oscillator wave function for  ${}^{12}\text{C}$  and the quasi-particle Lagrange Method of [13] for  ${}^{56}\text{Fe}$ . For the description of the  $eN$  interaction, the inelastic form factor parameterization of Ref. [14] and the dipole elastic form-factors have been used. These calculations are in reasonable agreement with existing  $A(e, e')X$  experimental data from SLAC [15] and from Jefferson Lab Hall C [16].

The ratios in Fig. 3 show a nice plateau starting from  $x_B > 1.5$  for both nuclei and all  $Q^2$ . The experimentally obtained ratio in the scaling region can be used to determine the relative probability of finding correlated  $NN$  pairs in different nuclei. However one needs to take into account two main factors: first the final state interactions of a nucleon with the residual system, and second the  $NN$  pair center-of-mass motion.

In the SRC model, FSI do not destroy the scaling behavior of the ratio,  $R$ . Indeed, in the light-cone approximation of the SRC model, if the invariant mass of the final  $NN$  system is sufficiently large,  $\sqrt{(q + m_D)^2 - m_D^2} > 50\text{-}100$  MeV, then the scattering amplitude will depend mainly on the light-cone fraction of the interacting nucleon's momentum  $\alpha = (E - p_z)/M$ , and has only a weak dependence on the conjugated variables  $E + p_z$  and  $p_t$  [6, 17, 18]. As a result, the closure approximation can be applied in the light-cone reference frame, allowing us to sum over all final states and use the fact that this sum is normalized to unity. After using the closure approximation the inclusive cross section will depend on the light-cone momentum distribution of the nucleon in the nucleus, integrated over the transverse momentum of the nucleon,  $\rho_A(\alpha)$  [5]. Thus, within the light cone description the Eq.(4) measures the ratio of  $\rho_A(\alpha)$  for nuclei  $A_1$  and  $A_2$  in the high-momentum range of the target nucleon.

In the lab frame description (in the virtual nucleon approach), however, the closure approximation cannot be applied for large values of interacting nucleon momenta, and FSI should be calculated explicitly (see *e.g.* Ref. [17]). Within the SRC model at high recoil momenta, FSI are dominated by the rescattering of the knocked-out nucleon with the correlated nucleon in the SRC [6, 17]. Therefore, FSI will be localized in SRC, and will cancel in the ratio  $R$ . As a result, Eq.(4) at  $x_B > x_B^0$  could be related to the ratio of high-momentum part of nucleon-momentum distributions in  $A_1$  and  $A_2$  nuclei [17].

Having an underlying model of the nuclear spectral functions, one can relate the measured ratios in Eq. (4) to the SRC properties of the nuclear wave function. Within the spectral function model [1], in which correlated nucleon pair is assumed at rest with the nucleon momentum distribution in pair identical to that in deuteron, the ratio in Eq. (4) could be directly related to the per-nucleon SRC probability in nucleus  $A$  relative to deuteron,  $a_2(A)$ . In models of the nuclear spectral function [19] in which two-nucleon correlations are moving in the mean field of the spectator  $A - 2$  system, the analysis of Eq. (4) will yield slightly smaller values for  $a_2(A)$ . Calculations by Ciofi degli Atti [20] indicate that this motion does not affect the scaling but can decrease the extracted  $a_2(A)$  for  ${}^{56}\text{Fe}$  by up to 20%. However it is important to emphasize that since both approximations predict similar (light cone) momentum distributions, both models lead to a similar ratio of the light-cone spectral functions and the overall probability of high-momentum nucleons



remains practically the same.

One can summarize the predictions of the SRC model for the ratios of the inclusive cross sections from different nuclei as follows (see Fig. 3):

- Scaling ( $x_B$  independence) is expected for  $Q^2 \geq 1$  (GeV/c)<sup>2</sup> and  $x_B^0 \leq x_B < 2$  where  $x_B^0$  is the threshold for high recoil momentum.
- No scaling is expected for  $Q^2 < 1$  (GeV/c)<sup>2</sup>.
- For  $x_B \leq x_B^0$  the ratios should have a minimum at  $x_B = 1$  and should grow with  $x_B$  since heavy nuclei have a broader momentum distribution than light nuclei for  $p < 0.3$  GeV/c.
- The onset of scaling depends on  $Q^2$ ;  $x_B^0$  should decrease with increasing  $Q^2$ .
- In the scaling regime, the ratios should be independent of  $Q^2$ .
- In the scaling regime the ratios should depend only weakly on  $A$  for  $A \geq 10$ . This reflects nuclear saturation.
- Ratios in the scaling regime are proportional to the ratios of the two-nucleon SRC probabilities in the two nuclei.

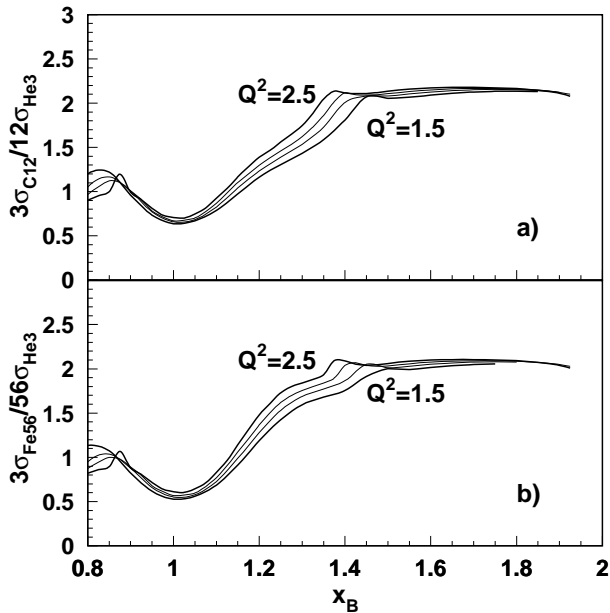


FIG. 3: SRC Model predictions for the normalized inclusive cross section ratio as a function of  $x_B$  for several values of  $Q^2$  (in (GeV/c)<sup>2</sup>). Note the scaling behavior predicted for  $x_B > 1.4$ . a) <sup>12</sup>C to <sup>3</sup>He, b) <sup>56</sup>Fe to <sup>3</sup>He.

Another possible mechanism for inclusive ( $e, e'$ ) scattering at  $x_B > 1$  is virtual photon absorption on a single nucleon followed by  $NN$  rescattering [21, 22]. Benhar

*et al.* [21] use the nuclear spectral function in the lab system and calculate the FSI using a correlated Glauber approximation (CGA), in which the initial momenta of the re-scattered nucleons are neglected. In this model the cross section at  $x_B > 1$  originates mainly from FSI and therefore the cross section ratios will not scale. This model predicts that these ratios also depend on  $Q^2$ , since it includes a noticeable reduction of FSI in order to agree with the data at  $Q^2 \geq 2$  (GeV/c)<sup>2</sup>. Benhar *et al.* attribute this reduction in FSI to color transparency effects [35]. The requirement of large color transparency effects also results in a strong  $A$  dependence of the ratio since the amount of the FSI suppression depends on the number of nucleons participating in the rescattering.

The main predictions of the CGA model for the nuclear cross section ratios are as follows:

- No scaling is predicted for  $Q^2 \geq 1$  (GeV/c)<sup>2</sup> and  $x_B < 2$ .
- The nuclear ratios should vary with  $Q^2$ .
- The ratios should depend on  $A$ .
- The model is not applicable below  $Q^2 = 1$  (GeV/c)<sup>2</sup>.

Thus, measuring the ratios of inclusive ( $e, e'$ ) scattering at  $x_B > 1$  and  $Q^2 > 1$  (GeV/c)<sup>2</sup> will yield important information about the reaction dynamics. If scaling is observed, then the dominance of the SRC in the nuclear wave function is manifested and the measured ratios will contain information about the probability of two-nucleon short range correlations in nuclei.

### III. EXPERIMENT

In this paper we present the first experimental studies of ratios of normalized, and acceptance- and radiative-corrected, inclusive yields of electrons scattered from <sup>4</sup>He, <sup>12</sup>C, <sup>56</sup>Fe, and <sup>3</sup>He measured under identical kinematical conditions.

The measurements were performed with the CEBAF Large Acceptance Spectrometer (CLAS) in Hall B at the Thomas Jefferson National Accelerator Facility. This is the first CLAS experiment with nuclear targets. Electrons with 2.261 and 4.461 GeV energies incident on <sup>3</sup>He, <sup>4</sup>He, <sup>12</sup>C, and <sup>56</sup>Fe targets have been used. We used helium liquefied in cylindrical target cells 1 cm in diameter and 4 cm long, positioned on the beam approximately in the center of CLAS. The solid targets were thin foils of <sup>12</sup>C (1mm) and <sup>56</sup>Fe (0.15 mm) positioned 1.5 cm downstream of the exit window of the liquid target. Data on solid targets have been taken with an empty liquid target cell.

The CLAS detector [24] consists of six sectors, each functioning as an independent magnetic spectrometer. Six superconducting coils generate a toroidal magnetic field primarily in the azimuthal direction. Each sector is instrumented with multi-wire drift chambers [25] and

time-of-flight scintillator counters [26] that cover the angular range from  $8^\circ$  to  $143^\circ$ , and, in the forward region ( $8^\circ < \theta < 45^\circ$ ), with gas-filled threshold Cherenkov counters (CC) [27] and lead-scintillator sandwich-type electromagnetic calorimeters (EC) [28]. Azimuthal coverage for CLAS is limited only by the magnetic coils, and is approximately 90% at large polar angles and 50% at forward angles. The CLAS was triggered on scattered electrons by a CC-EC coincidence at 2.2 GeV and by the EC alone with a  $\approx 1$  GeV electron threshold at 4.4 GeV.

For our analysis, electrons are selected in the kinematical region  $Q^2 > 0.65$  (GeV/c) $^2$  and  $x_B > 1$  where the contribution from the high-momentum components of the nuclear wave function should be enhanced. We also re-

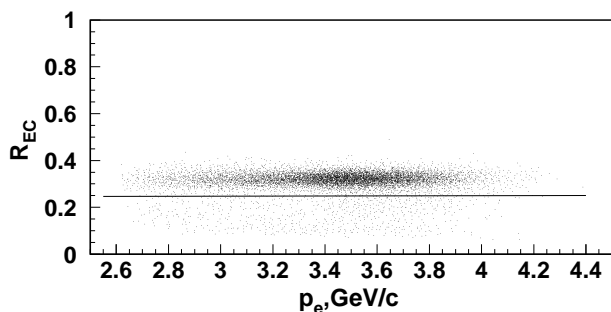


FIG. 4: The ratio ( $R_{EC}$ ) of energy deposited in the CLAS electromagnetic calorimeter (EC) to the electron momentum  $p_e$  as a function of  $p_e$  at beam energy 4.461 GeV. The line at  $R_{EC} \approx 0.25$  is located 3 standard deviations below the mean, as determined by measurements at several values of  $p_e$ . This cut was used to identify electrons.

quire that the energy transfer,  $\nu$ , should be  $> 300$  MeV (the characteristic missing energy for SRC is  $\sim 260$  MeV [1]). In this region one expects that inclusive  $A(e, e')$  scattering will proceed through the interaction of the incoming electron with a correlated nucleon in a SRC.

### A. Electron Identification

Electrons were selected in the fiducial region of the CLAS sectors. The fiducial region is a region of azimuthal angle, for a given momentum and polar angle, where the electron detection efficiency is constant. Then a cut on the ratio of the energy deposited in the EC to the measured electron momentum  $p_e$  ( $R_{EC}$ ) was used for final selection. In Fig. 4  $R_{EC}$  vs.  $p_e$  for the  $^{56}\text{Fe}$  target at 4.4 GeV is shown. The lines shows the applied cut at  $R_{EC} \approx 0.25$  which is located 3 standard deviations below the mean as determined by measurements at several values of  $p_e$ . A Monte Carlo simulation showed that these cuts reduce the  $A(e, e')$  yield by less than 0.5%.

We estimated the  $\pi^-$  contamination in the electron sample for a wide angular range using the photo-electron distributions in the CLAS Cherenkov counters. We found that for  $x_B > 1$  this is negligible.

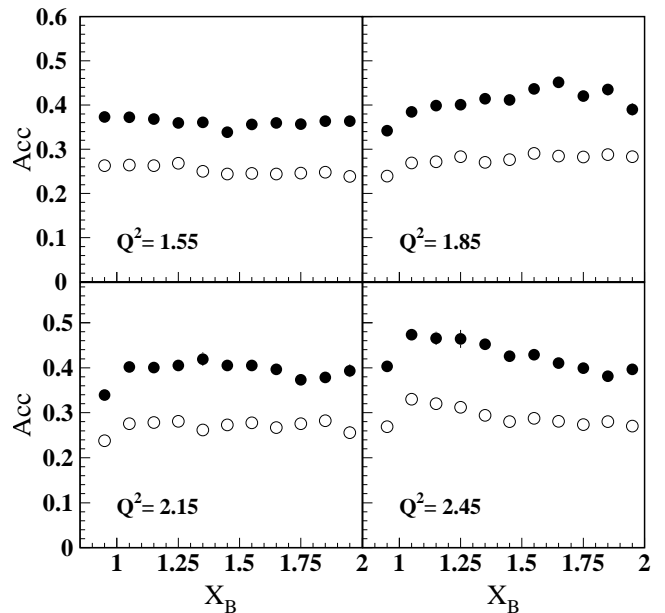


FIG. 5: The acceptance correction factors as a function of  $x_B$ .  $\bullet$   $^3\text{He}$ ,  $\circ$   $^{12}\text{C}$ .  $Q^2$  are in (GeV/c) $^2$ .

### B. Acceptance Corrections

We used the Monte Carlo techniques to determine the electron acceptance correction factors. Two iterations were done to optimize the cross section model for this purpose. In the first iteration we generated events using the SRC model [11] and determined the CLAS detector response using the GEANT-based CLAS simulation program, taking into account “bad” or “dead” hardware channels in various components of CLAS, as well as realistic position resolution for the CLAS drift chambers. We then used the CLAS data analysis package to reconstruct these events using the same electron identification criteria that was applied to the real data. The acceptance correction factors were found as the ratios of the number of reconstructed and simulated events in each kinematic bin. Then the acceptance corrections were applied to the data event-by-event, i.e. each event was weighted by the acceptance factor obtained for the corresponding ( $\Delta x_B, \Delta Q^2$ ) kinematic bin and the cross sections were calculated as a function of  $x_B$  and  $Q^2$ . For the second iteration the obtained cross sections were fitted and the fit-functions were used to generate a new set of data, and the process was repeated. Fig. 5 shows the electron acceptance factors after the second iteration for liquid ( $^3\text{He}$ ) and solid ( $^{12}\text{C}$ ) targets. We used the difference between the iterations as the uncertainty in the acceptance correction factor. Note that the acceptance for the carbon target is smaller than for the helium target. This is due to the closer location of the solid targets to the CLAS coils, which limit azimuthal angular coverage of the detectors.

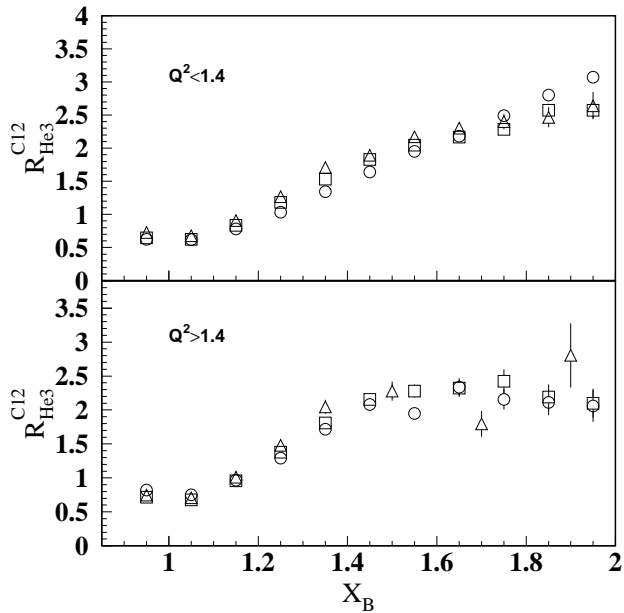


FIG. 6:  $R_{\text{He3}}^{\text{C12}}$ , the per-nucleon yield ratios for  $^{12}\text{C}$  to  $^3\text{He}$ . a)  $\circ$   $0.65 < Q^2 < 0.85$ ;  $\square$   $0.9 < Q^2 < 1.1$ ;  $\triangle$   $1.15 < Q^2 < 1.35$  ( $\text{GeV}/c$ ) $^2$ , all at incident energy 2.261 GeV. b)  $\circ$   $1.4 < Q^2 < 1.6$  ( $\text{GeV}/c$ ) $^2$  and at incident energy 2.261 GeV;  $\square$   $1.4 < Q^2 < 2.0$ ;  $\triangle$   $2.0 < Q^2 < 2.6$  ( $\text{GeV}/c$ ) $^2$ , both at incident energy 4.461 GeV. Statistical errors are shown only.

### c. Radiative Corrections

The cross section ratios were corrected for radiative effects. The radiative correction for each target as a function of  $Q^2$  and  $x_B$  was calculated as the ratio

$$C_{\text{rad}}(x_B, Q^2) = \frac{d\sigma^{\text{rad}}(x_B, Q^2)}{d\sigma^{\text{norad}}(x_B, Q^2)}, \quad (5)$$

where  $d\sigma^{\text{rad}}(x_B, Q^2)$  and  $d\sigma^{\text{norad}}(x_B, Q^2)$  are the radiatively corrected and uncorrected theoretical cross sections, respectively. The cross sections have been calculated using [11].

## IV. RESULTS

We constructed ratios of normalized, acceptance- and radiative-corrected inclusive electron yields on nuclei  $^4\text{He}$ ,  $^{12}\text{C}$  and  $^{56}\text{Fe}$  divided the yield on  $^3\text{He}$  in the range of kinematics  $1 < x_B < 2$ . Assuming that electron detection efficiency from different targets is the same, these ratios, weighted by atomic number, are equivalent to the ratios of cross sections in Eq. 4.

The normalized yields for each  $x_B$  and  $Q^2$  bin have been calculated as:

$$\frac{dY}{dQ^2 dx_B} = \frac{N_{e'}}{\Delta Q^2 \Delta x_B N_e N_T} \cdot \frac{1}{\text{Acc}} \quad (6)$$

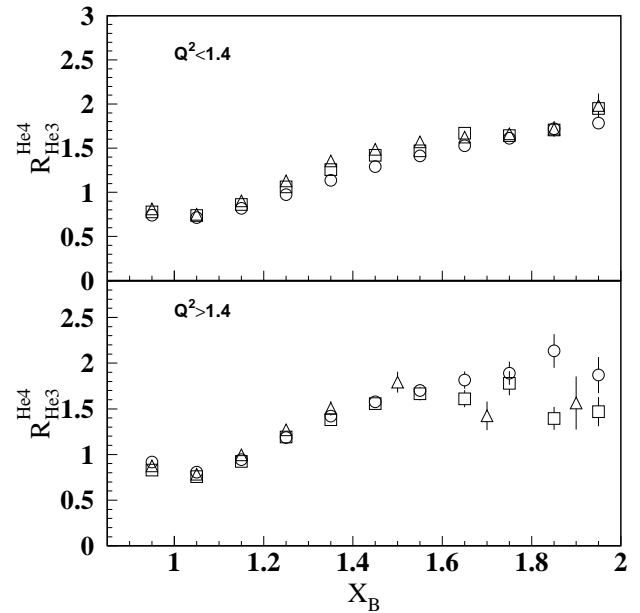


FIG. 7: The same as Fig. 6 for  $^4\text{He}$ .

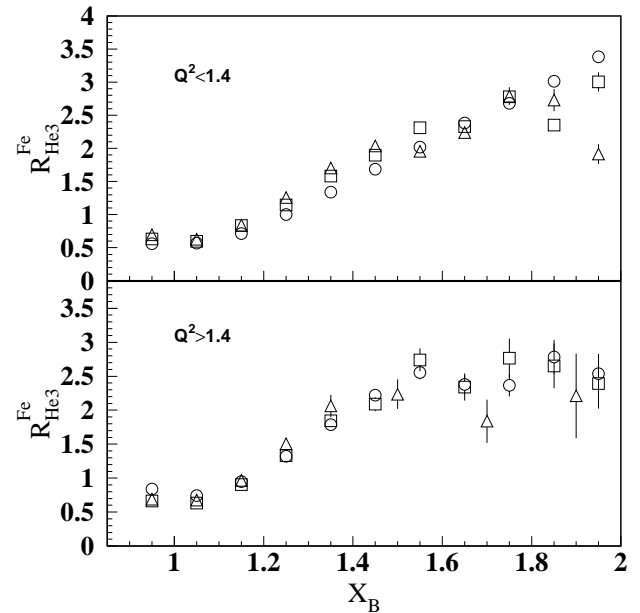


FIG. 8: The same as Fig. 6 for  $^{56}\text{Fe}$ .

where  $N_e$  and  $N_T$  are the number of electrons and target nuclei, respectively,  $\text{Acc}$  is the acceptance correction factor, and  $\Delta Q^2$  and  $\Delta x_B$  are the bin sizes in  $Q^2$  and in  $x_B$ , respectively. Since electron detection efficiency in CLAS is expected to be  $> 96\%$ , we compare obtained yields with radiated cross sections calculated by Ref. [11] code. Within systematic uncertainties (see below) the satisfactory agreement has been found between our results and the calculations from Ref. [11] that were tuned on SLAC [15] and Jefferson Lab Hall C [16] data.

The ratios  $R_{3He}^A$ , also corrected for radiative effects, are defined as:

$$R_{3He}^A(x_B) = \frac{3\mathcal{Y}^A}{A\mathcal{Y}^{3He}} \frac{C_{Rad}^A}{C_{Rad}^{3He}}, \quad (7)$$

where  $\mathcal{Y}$  is the normalized yield in a given  $(x_B, Q^2)$  bin, and  $C_{Rad}$  is the radiative correction factor from Eq. 5 for each nucleus.

Fig. 6 shows these ratios for  $^{12}C$  at several values of  $Q^2$ . Figs. 7 and 8 show these ratios for  $^4He$  and  $^{56}Fe$ , respectively. These data have the following important characteristics:

- There is a clear  $Q^2$  evolution of the shape of ratios:
  - At low  $Q^2$  ( $Q^2 < 1.4$  (GeV/c) $^2$ ),  $R_{3He}^A(x_B)$  increases with  $x_B$  in the entire  $1 < x_B < 2$  range (see Figs. 6a – 8a).
  - At high  $Q^2$  ( $Q^2 \geq 1.4$  (GeV/c) $^2$ )  $R_{3He}^A(x_B)$  is independent of  $x_B$  for  $x_B > x_B^0 \approx 1.5$ . (See Figs. 6b – 8b.)
- The value of  $R_{3He}^A(x_B)$  in the scaling regime is independent of  $Q^2$ .
- The value of  $R_{3He}^A(x_B)$  in the scaling regime for  $A > 10$  suggests a weak dependence on target mass.

### A. Systematic Errors

The systematic errors in this measurement are different for different targets and include uncertainties in:

- fiducial cut applied:  $\approx 1\%$ ;
- radiative correction factors:  $\approx 2\%$ ;
- target densities and thicknesses:  $\approx 0.5\%$  and  $1.0\%$  for solid targets;  $0.5\%$  and  $3.5\%$  for liquid targets, respectively.
- acceptance correction factors ( $Q^2$  dependent): between 2.2 and 4.0% for solid targets and between 1.8 and 4.3% for liquid targets.

Some of systematic uncertainties will cancel out in the yield ratios. For the  $^3He/^4He$  ratio, all uncertainties except those on the beam current and the target density divide out, giving a total systematic uncertainty of 0.7%. For the solid-target to  $^3He$  ratios, only the electron detection efficiency cancels. The quadratic sum of the other uncertainties is between 5% and 7%, depending on  $Q^2$ . The systematic uncertainties on the ratios for all targets and  $Q^2$  are presented in Table I.

| $Q^2$            | 1.55 | 1.85 | 2.15 | 2.45 |
|------------------|------|------|------|------|
| $\delta R^A$     | 7.1  | 5.8  | 4.9  | 5.1  |
| $\delta R^{He4}$ | 0.7  | 0.7  | 0.7  | 0.7  |

TABLE I: Systematic uncertainties  $\delta R^A$  and  $\delta R^{He4}$  for the ratio of normalized inclusive yields  $R_{3He}^{C,Fe}$  and  $R_{3He}^{4He}$  respectively, in %.  $Q^2$  in (GeV/c) $^2$ , and  $\Delta Q^2 = \pm 0.15$  (GeV/c) $^2$ .

### B. Probabilities of Two-Nucleon Short Range Correlations in Nuclei

Our data are clearly consistent with the predictions of the  $NN$  SRC model. The obtained ratios,  $R_{3He}^A$ , for  $1.4 < Q^2 < 2.6$  (GeV/c) $^2$  region are shown in Table II as a function of  $x_B$ . Fig. 9 shows these ratios for the  $^{12}C$  and  $^{56}Fe$  targets together with the SRC calculation results using of Ref. [11] which used the estimated scaling factors,  $a_2(A)$ , (per-nucleon probability of  $NN$  SRC in nucleus A) from Ref. [6]. Good agreement between our data and calculation is seen. Note that one of the goals of the present paper is to determine these factors more precisely (see below).

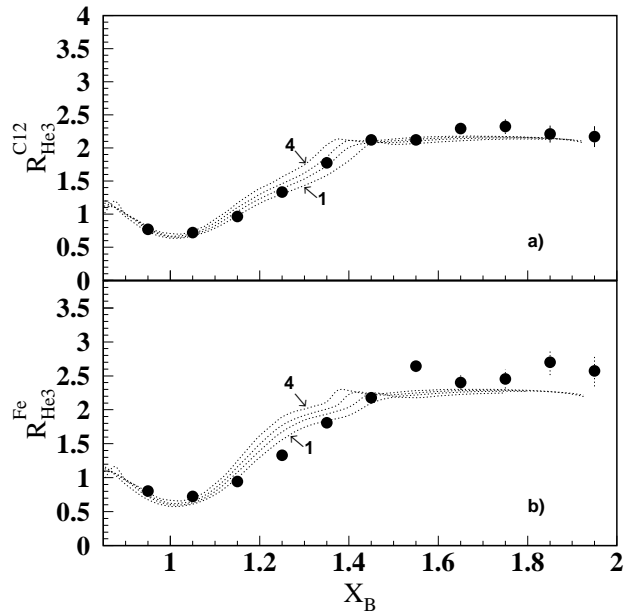


FIG. 9:  $R_{3He}^A(x_B)$  as a function of  $x_B$  for  $1.4 < Q^2 < 2.6$  (GeV/c) $^2$ , statistical errors are shown only. Curves are SRC model predictions for different  $Q^2$  in the range 1.4 (GeV/c) $^2$  (curve 1) to 2.6 (GeV/c) $^2$  (curve 4), respectively, for a)  $^{12}C$ , b)  $^{56}Fe$ .

Experimental data in the scaling region can be used to estimate the relative probabilities of  $NN$  SRC in nuclei compared to  $^3He$ . According to Ref. [1] the ratio of these



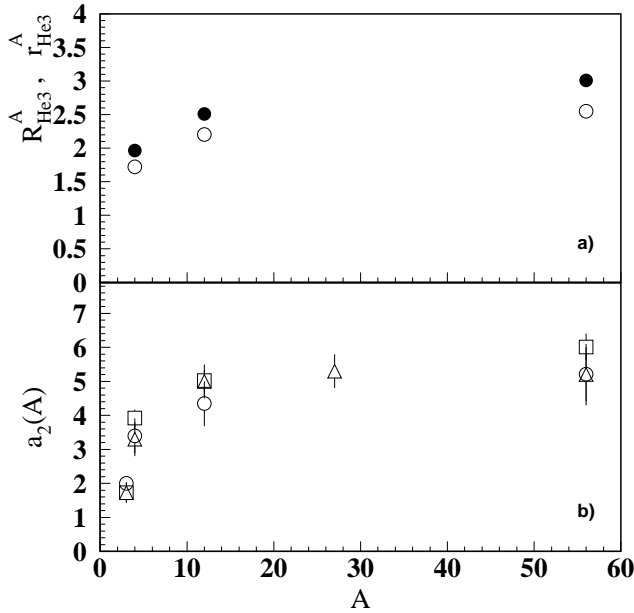


FIG. 10: a)  $R_{He3}^A$  ( $\circ$ ) and  $r_{He3}^A$  ( $\bullet$ ) versus  $A$ . b)  $a_2(A)$  versus  $A$ .  $\circ$  -  $a_2(A)$  is obtained from Eq.(10) using the experimental value of  $a_2(3)$  Ref. [6];  $\square$  -  $a_2(A)$  is obtained using the theoretical value of  $a_2(3)$ . For errors shown see caption of Table III.  $\triangle$  - data from Ref. [6].

probabilities is proportional to:

$$r_{He3}^A = \frac{(2\sigma_p + \sigma_n)\sigma_A}{(Z\sigma_p + N\sigma_n)\sigma_{He3}}, \quad (8)$$

where  $\sigma_A$  and  $\sigma_{He3}$  are the  $A(e, e')$  and  ${}^3\text{He}(e, e')$  inclusive cross sections respectively.  $\sigma_p$  and  $\sigma_n$  are the electron-proton and electron-neutron elastic scattering cross sections respectively.  $Z$  and  $N$  are the number of protons and neutrons in nucleus  $A$ . Using Eq. (4) the ratio of Eq. (8) can be related to the experimentally measured ratios  $R_{He3}^A$  as

$$r_{He3}^A = R_{He3}^A(x_B, Q^2) \times \frac{A(2\sigma_p + \sigma_n)}{3(Z\sigma_p + N\sigma_n)} \quad (9)$$

To obtain the numerical values for  $r_{He3}^A$  we calculated the second factor in Eq. (9) using parameterizations for the neutron and proton form factors [29, 30, 31, 32]. We found the average values of these factors to be  $1.14 \pm 0.02$  for  ${}^4\text{He}$  and  ${}^{12}\text{C}$ , and  $1.18 \pm 0.02$  for  ${}^{56}\text{Fe}$ . Note that these factors vary slowly over our  $Q^2$  range. For  $r_{He3}^A$  calculations the experimental data were integrated over  $Q^2 > 1.4$  (GeV/c) $^2$  and  $x_B > 1.5$  for each nucleus. The ratio of integrated yields,  $R_{He3}^A(x_B)$ , are presented in the first column of Table III and in Fig. 10a (rectangles). The ratios  $r_{He3}^A$  are shown in the second column of Table III and by the circles in Fig. 10a. One can see that the ratios  $r_{He3}^A$  are 2.5 - 3.0 for  ${}^{12}\text{C}$  and  ${}^{56}\text{Fe}$ , and approximately 1.95 for  ${}^4\text{He}$ .

| $X_B$           | ${}^4\text{He}$  | ${}^{12}\text{C}$ | ${}^{56}\text{Fe}$ |
|-----------------|------------------|-------------------|--------------------|
| $0.95 \pm 0.05$ | $0.86 \pm 0.004$ | $0.77 \pm 0.003$  | $0.80 \pm 0.004$   |
| $1.05 \pm 0.05$ | $0.78 \pm 0.004$ | $0.72 \pm 0.003$  | $0.72 \pm 0.004$   |
| $1.15 \pm 0.05$ | $0.94 \pm 0.006$ | $0.96 \pm 0.006$  | $0.94 \pm 0.007$   |
| $1.25 \pm 0.05$ | $1.19 \pm 0.012$ | $1.33 \pm 0.012$  | $1.33 \pm 0.015$   |
| $1.35 \pm 0.05$ | $1.41 \pm 0.021$ | $1.77 \pm 0.025$  | $1.81 \pm 0.030$   |
| $1.45 \pm 0.05$ | $1.58 \pm 0.033$ | $2.12 \pm 0.044$  | $2.17 \pm 0.055$   |
| $1.55 \pm 0.05$ | $1.71 \pm 0.049$ | $2.12 \pm 0.059$  | $2.64 \pm 0.087$   |
| $1.65 \pm 0.05$ | $1.70 \pm 0.063$ | $2.29 \pm 0.085$  | $2.40 \pm 0.109$   |
| $1.75 \pm 0.05$ | $1.85 \pm 0.089$ | $2.32 \pm 0.110$  | $2.45 \pm 0.139$   |
| $1.85 \pm 0.05$ | $1.65 \pm 0.100$ | $2.21 \pm 0.128$  | $2.70 \pm 0.190$   |
| $1.95 \pm 0.05$ | $1.71 \pm 0.124$ | $2.17 \pm 0.157$  | $2.57 \pm 0.227$   |

TABLE II: The ratios,  $R_{He3}^A$ , measured in  $1.4 < Q^2 < 2.6$  (GeV/c) $^2$  interval. Errors are statistical only.

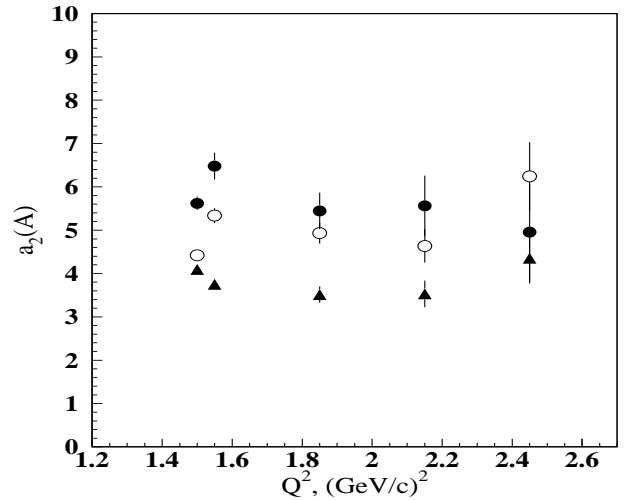


FIG. 11:  $Q^2$  - dependences of  $a_2(A)$  parameters obtained by multiplying  $r_{He3}^A$  ( $= \frac{a_2(A)}{a_2(3)}$ ) with the theoretical values of  $a_2(3)$ . For errors shown see caption of Table III.  $\blacktriangle$   ${}^4\text{He}$ ,  $\circ$   ${}^{12}\text{C}$  and  $\bullet$   ${}^{56}\text{Fe}$ .

The per-nucleon SRC probability in nucleus  $A$  relative to  ${}^3\text{He}$  is proportional to  $r_{He3}^A \sim a_2(A)/a_2(3)$ , where  $a_2(A)$  and  $a_2(3)$  are the per-nucleon probability of SRC relative to deuterium for nucleus  $A$  and  ${}^3\text{He}$ . As was discussed earlier, the direct relation of  $r_{He3}^A$  to the per-nucleon probabilities of SRC has an uncertainty of up to 20% due to pair center-of-mass motion. Within this uncertainty, we will define the per-nucleon SRC probabilities of nuclei relative to deuterium as:

$$a_2(A) = r_{He3}^A \cdot a_2(3) \quad (10)$$

Two values of  $a_2(3)$  have been used to calculate  $a_2(A)$ . First is the experimentally obtained value from Ref. [6],  $a_2(3) = 1.7 \pm 0.3$ , and the second the value from the calculation using the wave function for deuterium and  ${}^3\text{He}$ ,

$a_2(3)=2\pm 0.1$ . Similar results were obtained in Ref. [33].

|                    | $R_{3He}^A(x_B)$ | $r_{3He}^A$     | $a_2(A)^{exp}$  | $a_2(A)^{theor}$ |
|--------------------|------------------|-----------------|-----------------|------------------|
| ${}^4\text{He}$    | $1.72 \pm 0.03$  | $1.96 \pm 0.05$ | $3.39 \pm 0.51$ | $3.93 \pm 0.24$  |
| ${}^{12}\text{C}$  | $2.20 \pm 0.04$  | $2.51 \pm 0.06$ | $4.34 \pm 0.66$ | $5.02 \pm 0.31$  |
| ${}^{56}\text{Fe}$ | $2.54 \pm 0.06$  | $3.00 \pm 0.08$ | $5.21 \pm 0.79$ | $6.01 \pm 0.38$  |

TABLE III:  $R_{3He}^A(x_B)$  is the ratio of normalized ( $e, e'$ ) yields for nucleus  $A$  to  ${}^3\text{He}$ .  $r_{3He}^A$  is the relative per-nucleon probability of SRC for the two nuclei. Both values are obtained from the scaling region ( $Q^2 > 1.4$  (GeV/c) $^2$  and  $x_B > 1.5$ ).  $a_2(A)^{exp}$  and  $a_2(A)^{theor}$  are the  $a_2(A)$  parameters obtained by multiplying  $r_{3He}^A$  ( $=\frac{a_2(A)}{a_2(3)}$ ) with the experimental and/or theoretical values of  $a_2(3)$ . The  $R_{3He}^A(x_B)$  ratios include statistical errors only. Errors of  $r_{3He}^A$  include also uncertainties in the second factor in Eq.(9). Errors in  $a_2(A)^{exp}$  and  $a_2(A)^{theor}$  also include uncertainties in the corresponding values of  $a_2(3)$ . For systematic uncertainties see Table I. There is an overall theoretical uncertainty of 20% in converting these ratios into SRC probabilities.

The per-nucleon probability of SRC for nucleus  $A$  relative to deuterium is shown in the third and fourth columns of Table III and in Fig. 10b. The uncertainties in existing  $a_2(3)$  are included in the errors for  $a_2(A)$ . The results from Ref. [6] are shown as well. One can see that  $a_2(A)$  changes significantly from  $A = 4$  to  $A = 12$  but does not change significantly for  $A \geq 12$ . There are approximately 5.5 times as much SRC for  $A \geq 12$  than for deuterium, and approximately 3.5 times as much SRC for  ${}^4\text{He}$  as for deuterium. These results are consistent with the analysis of the previous SLAC ( $e, e'$ ) data [6]. They are also consistent with calculations of Ref. [33].

Fig. 11 shows the measured  $Q^2$  dependence of the relative SRC probability,  $a_2(A)$ , which appears to be  $Q^2$  independent for all targets.

## V. SUMMARY

The  $A(e, e')$  inclusive electron scattering cross section ratios of  ${}^4\text{He}$ ,  ${}^{12}\text{C}$ , and  ${}^{56}\text{Fe}$  to  ${}^3\text{He}$  have been measured for the first time under identical kinematical conditions.

It is shown that:

1. These ratios are independent of  $x_B$  (scale) for  $x_B > 1.5$  and  $Q^2 > 1.4$  (GeV/c) $^2$ , *i.e.* for high recoil momentum. The ratios do not scale for  $Q^2 < 1.4$  (GeV/c) $^2$ .
2. These ratios in the scaling region are independent of  $Q^2$ , and approximately independent of  $A$  for  $A \geq 12$
3. These features were predicted by the Short Range Correlation model of inclusive  $A(e, e')$  scattering at large  $x_B$ , and consistent with the kinematical expectation that two nucleon short range correlations are dominating in the nuclear wave function at  $p_m \gtrsim 300$  MeV/c [6].
4. The observed scaling shows that momentum distributions at high-momenta have the same shape for all nuclei and differ only by a scale factor.
5. Using the SRC model, the values of the ratios in the scaling region were used to derive the relative probabilities of SRC in nuclei compared to deuterium. The per-nucleon probability of Short Range Correlations in nuclei relative to deuterium is  $\approx 3.5$  times larger for  ${}^4\text{He}$  and 5.0 - 5.5 times larger for  ${}^{12}\text{C}$  and  ${}^{56}\text{Fe}$ .

## ACKNOWLEDGMENT

We acknowledge the efforts of the staff of the Accelerator and Physics Divisions (especially the Hall B target group) at Jefferson Lab in their support of this experiment. We also acknowledge useful discussions with D. Day and E. Piasecki. This work was supported in part by the U.S. Department of Energy, the National Science Foundation, the French Commissariat a l'Energie Atomique, the French Centre National de la Recherche Scientifique, the Italian Istituto Nazionale di Fisica Nucleare, and the Korea Research Foundation. U. Thoma acknowledges an "Emmy Noether" grand from the Deutsche Forschungsgemeinschaft. The Southeastern Universities Research Association (SURA) operates the Thomas Jefferson National Accelerator Facility for the United States Department of Energy under contract DE-AC05-84ER40150.

- 
- |  |  |
|--|--|
| <p>[1] L.L. Frankfurt and M.I. Strikman, Phys. Rep. <b>76</b>, 215 (1981); , Phys. Rep. <b>160</b>, 235 (1988).</p> <p>[2] T.W. Donnelly and I. Sick, Phys. Rev. C <b>60</b>, 065502 (1999);</p> <p>[3] J. Arrington, <i>et al.</i>, Phys. Rev. Lett. <b>82</b>, 2056 (1999).</p> <p>[4] C. Ciofi degli Atti, Phys. Rev. C <b>53</b>, 1689, (1996).</p> <p>[5] L. Frankfurt and M. Strikman, in <i>Electromagnetic Interactions with Nuclei</i>, edited by B. Frois and I. Sick (World Scientific, Singapore, 1991).</p> | <p>[6] L.L. Frankfurt, M.I. Strikman, D.B. Day, M.M. Sargsyan, Phys. Rev. C <b>48</b>, 2451 (1993).</p> <p>[7] W.P. Schutz <i>et al.</i>, Phys. Rev. Lett. <b>38</b>, 8259 (1977).</p> <p>[8] S. Rock <i>et al.</i>, Phys. Rev. Lett. <b>49</b>, 1139 (1982).</p> <p>[9] R.G. Arnold <i>et al.</i>, Phys. Rev. Lett. <b>61</b>, 806 (1988).</p> <p>[10] D. Day <i>et al.</i>, Phys. Rev. Lett. <b>59</b>, 427 (1979).</p> <p>[11] M. Sargsian, CLAS-NOTE 90-007 (1990).</p> <p>[12] R. Machleidt, Phys. Rev. C <b>63</b>, 024001 (2001).</p> <p>[13] M.V. Zverev and E.E. Saperstein, Yad. Fiz. <b>43</b>, 304</p> |
|--|--|

- (1986).
- [14] A. Bodek *et al.*, Phys. Rev. D **20**, 1471 (1979).
  - [15] D. Day *et al.*, Phys. Rev. Lett. **43**, 1143 (1979).
  - [16] Th.C. Petitjean, Inaugural-Dissertation, Basel, 2000.
  - [17] L.L. Frankfurt, M.M. Sargsian, and M.I. Strikman, Phys. Rev. C **56**, 1124 (1997).
  - [18] M.M. Sargsian, Dissertation, Yerevan, 1993 and Int. J. Mod. Phys. E **10**, 405 (2001).
  - [19] C. Ciofi degli Atti, S. Simula, L. L. Frankfurt and M. I. Strikman, Phys. Rev. C **44**, 7 (1991).
  - [20] C. Ciofi degli Atti, Private Communication.
  - [21] O. Benhar *et al.*, Phys. Rev. C **44**, 2328 (1991).
  - [22] O. Benhar *et al.*, Phys. Lett. B **343**, 47 (1995).
  - [23] K. Garrow *et al.*, Phys. Rev. C **66**, 044613 (2002).
  - [24] CEBAF Hall B Conceptual Design Report, April 1990.
  - [25] M.D. Mestayer *et al.*, Nucl. Inst. and Meth. **A449**, 81 (2000).
  - [26] E.S. Smith *et al.*, Nucl. Inst. and Meth. **A432**, 265 (1999).
  - [27] G. Adams *et al.*, Nucl. Inst. and Meth. **A465**, 414 (2001).
  - [28] M. Amarian *et al.*, Nucl. Inst. and Meth. **A460**, 239 (2001).
  - [29] I.G. Aznauryan, Private Communication.
  - [30] Kees De Jager, JLAB-PHY-00-01, 2001.
  - [31] P.E. Bosted *et al.*, Phys. Rev C **51**, 409 (1995).
  - [32] M.L. Miller *et al.*, Phys. Rev. Lett. **84**, 1398 (2000).
  - [33] J.L. Forest *et al.*, Phys. Rev. C **54**, 646 (1996).
  - [34] Hereafter, by the ratio of the cross sections we will mean the ratios of the cross sections weighted by  $A$ . We will separately discuss effects due to  $\sigma_{ep} > \sigma_{en}$  that are important for  ${}^3\text{He}$  due to  $Z$  not equal to  $N$ .
  - [35] So far no color transparency effects are observed in  $A(e, e'p)X$  reactions at  $Q^2 \leq 8$  (GeV/c)<sup>2</sup> [23].